

A large-scale R-matrix calculation for electron-impact excitation of the Ne^{2+} , O-like ion

B M McLaughlin^{1,2†}, Teck-Ghee Lee³, J A Ludlow³, E Landi⁴, S D Loch³, M S Pindzola³ and C P Ballance^{3‡},

¹Centre for Theoretical Atomic, Molecular and Optical Physics (CTAMOP), School of Mathematics and Physics, The David Bates Building, 7 College Park, Queen's University Belfast, Belfast BT7 1NN, UK

²Institute for Theoretical Atomic and Molecular Physics, Harvard Smithsonian Center for Astrophysics, MS-14, Cambridge, MA 02138, USA

³Department of Physics, Auburn University, Auburn, AL 36849, USA

⁴Department of Atmospheric, Oceanic and Space Sciences, University of Michigan, Ann Arbor MI 48109, USA

Abstract.

The five JII levels within a np^2 or np^4 ground state complex provide an excellent testing ground for the comparison of theoretical line ratios with astrophysically observed values, in addition to providing valuable electron temperature and density diagnostics. The low temperature nature of the line ratios ensure that the theoretically derived values are sensitive to the underlying atomic structure and electron-impact excitation rates. Previous R-matrix calculations for the O-like Ne ion, Ne^{2+} , exhibit spurious structure in the cross sections at higher electron energies, which may affect Maxwellian averaged rates even at low temperatures. Furthermore, there is an absence of comprehensive excitation data between the excited states that may provide newer diagnostics to compliment the more established lines discussed in this paper. To resolve these issues, we present both a small-scale 56-level Breit-Pauli (BP) calculation and a large-scale 554 levels R-matrix Intermediate Coupling Frame Transformation (ICFT) calculation that extends the scope and validity of earlier JAJOM calculations both in terms of the atomic structure and scattering cross sections. Our results provide a comprehensive electron-impact excitation data set for all transitions to higher n - shells. The fundamental atomic data for this O-like ion is subsequently used within a collisional radiative framework to provide the intensity line ratios across a range of electron temperatures and densities of interest in astrophysical observations.

PACS numbers: 32.80F

Short title: Electron impact excitation of Ne^{2+} ions

Revised: J. Phys. B: At. Mol. & Opt. Phys: 30 October 2021

† Corresponding author, E-mail: b.mclaughlin@qub.ac.uk

‡ Corresponding author, E-mail: ballance@physics.auburn.edu

1. Introduction

Electron-impact excitation rates are a fundamental component of collisional radiative modelling. In particular, the excitation rates for O-like Ne (Ne^{2+}), the focus of this paper, are applicable in diagnosing the spectral lines not only from astrophysical observations but also from fusion plasma studies. It has been shown that transitions within the first five levels of an atom with the np^4 ground configuration can provide a valuable diagnostic of the electron temperature [1] and the electron density [2]. Recently, an updated electron-impact excitation calculation of Munoz *et al.* [3] for the $3s^23p^4$ ground state complex of O-like Ar (Ar^{2+}) found that the plasma diagnostics were particularly sensitive to near threshold resonances, and therefore, Ne^{2+} may offer a similar diagnostic potential, but without the high sensitivity to single near threshold resonance as found in the Ar^{2+} case.

Neon plays an important role in a variety of astrophysical phenomena, being the most abundant rare gas in the universe after helium. Forbidden Ne III lines have been observed in a variety of astrophysical plasmas. The lines at $36 \mu m$ and 3869 \AA , due to forbidden $^3P_0 \rightarrow ^3P_1$ and $^1D_2 \rightarrow ^3P_2$ transitions within the ground configuration, have been observed in H II regions by a number of authors [4, 5, 6, 7]. The Ne III 3869 \AA line is also present in Ne-rich filaments in the Supernova Cas A remnant [8, 9] and can be used to investigate the neon abundance and its spatial distribution throughout the remnant.

In terms of laboratory measurements, the identification of Ne III lines were reviewed by Persson *et al.* [10] and the low lying terms are depicted in Fig 1. The present R-matrix calculation now includes shells of sufficiently high principal quantum numbers for a direct comparison with significantly more of their listed lines. More recently, James and co-workers [11] measured electron-impact excitation cross sections for transitions in the far ultraviolet wavelength range between 1200 and 2700 \AA using an electron-ion impact collision chamber. Daw *et al.* [12] have measured a pair of lines within the ground-state complex. The spin forbidden line $^1S_0 \rightarrow ^3P_1$ and the quadrupole $^1S_0 \rightarrow ^1D_2$ line offer diagnostic potential. Finally, Fig 2 illustrates the transitions of interest in the planetary nebulae NGC 3918 [13] for Ne III. The wavelength of the astrophysically observed transitions are labelled in units of Angstroms.

An overview of the various theoretical models investigating electron impact excitation of Ne^{2+} is summarized in the introduction of McLaughlin and Bell [14]. This includes the work of Seaton [15, 16, 17] in the 1950s, and continues through a progression of the perturbative calculations (e.g., Coulomb-Born [18] and distorted wave [19] in 1960s-1970s) yet only for transitions within the $1s^22s^22p^4$ ground state complex. These were followed by early R-matrix calculations of Pradhan [20] and Butler and Mendoza [21] using a program of Saraph [22, 23] to transform LS-coupled K-matrices into level-level cross sections using the JAJOM code. This work included six states in the close coupling expansion and clearly illustrated the sensitivity of excitation rates when adopting either theoretically calculated or experimentally observed energy level values.

Between 1999 and 2001, McLaughlin and co-workers in a couple of papers [14, 24] extended this model to 28 LS terms or 56 levels arising from the following $1s^22s^22p^4, 2s2p^5, 2s^22p^33l(l=0-2), 2s^22p^34s$ configurations, with the extra $4\bar{p}, 4d$ orbitals used only as an improvement in the description of the target's states. However, as evident in Fig. 5 of Ref.[14] there is a breakdown in their calculation for the 28 terms

model, manifesting as broad unphysical 2 eV resonances in transitions from the 3P_0 ground state term. Unsurprisingly, this leads to corresponding unphysical increase in the effective collision strength (see Fig. 6 in Ref.[14]) at approximately $10^{4.5}$ Kelvin. We point out that a less elaborate six-level model does not exhibit the same problem as indicated in Ref.[14].

Therefore, it would not be unreasonable, given the increase in computational power over the last decade to pursue a full Breit-Pauli R-matrix calculation for the 56 levels under consideration that would resolve and correct this problem. However, our present studies revealed that the 6 configurations listed above, actually give rise to a possible 49 terms or 95 levels. This imbalance between the configuration-interaction of the target and those levels actually used in the close coupling expansion will give rise to secondary, but a less pronounced set of pseudo-resonances above 3 Rydbergs. Therefore, to correct and also expand the scope of Ne^{2+} R-matrix calculations currently in the literature we have carried out an Intermediate Coupling Frame Transformation (ICFT) [25] calculation for 554 levels. As illustrated in Ref.[3], the use of the ICFT method gives cross sections that are extremely close to a Breit-Pauli (BP) calculation if both employing the same target configurations.

The remainder of the paper is organized as follows. In section 2 we outline our small Breit-Pauli R-matrix and a large scale level ICFT R-matrix calculation used in the current study. Section 3, gives results for selected collision strengths and effective collision strengths and compares the BP and ICFT calculations. A small collisional radiative calculation is then performed in section 4, to predict observed astronomical line ratios. Finally, in the summary, we assess the impact of this now complete data set on the predictive modelling of Ne^{2+} line ratios.

2. Details of calculations

In the smaller R-matrix Breit-Pauli model, the atomic orbitals employed were generated from the atomic structure code CIV3 [26]; in which the orbitals were energy-optimized on the lowest 28 terms; details can be found in the earlier work of McLaughlin and co-workers [14, 24]. A subset of 28 LS terms constructed from the following configuration list; $1s^2 2s^2 2p^4$, $1s^2 2s 2p^5$, $1s^2 2s^2 2p^3 3l$ and $1s^2 2p^6$ give rise to 56 fine-structure levels which were used in the close-coupling expansion. Extra diffuse $4\bar{p}$ and $4\bar{d}$ pseudo-orbitals were used only to improve the target states, but also ensured a larger R-matrix box of 15.2 a.u. A total of forty basis orbitals were used to represent the continuum basis, easily spanning the energy range from threshold to 20 Rydbergs.

In the larger ICFT calculation, the target radial wavefunctions were generated using GASP (Graphical Autostructure Package) [27], which is a java front-end for the atomic-structure code AUTOSTRUCTURE [28]. The orbitals were generated within an Thomas-Fermi-Dirac-Amaldi potential, using slightly modified lambda scaling parameters as given by Landi and Bhatia [29]. Specifically we used $\lambda_{1s} = 1.0$, $\lambda_{2s} = 1.3$, $\lambda_{2p} = 1.09$, $\lambda_{3s} = 1.13$, $\lambda_{3p} = 1.15$, $\lambda_{3d} = 1.11$, $\lambda_{4s} = 1.12$, $\lambda_{4p} = 1.1$, $\lambda_{4d} = 1.11$ and $\lambda_{4f} = 1.06$. However, we are able to include all 24 configurations : $2s^2 2p^4$, $2s 2p^5$, $2p^6$, $2s^2 2p^3 3s$, $2s^2 2p^3 3p$, $2s^2 2p^3 3d$, $2s^2 2p^3 4s$, $2s^2 2p^3 4p$, $2s^2 2p^3 4d$, $2s^2 2p^3 4f$, $2s 2p^4 3s$, $2s 2p^4 3p$, $2s 2p^4 3d$, $2s 2p^4 4s$, $2s 2p^4 4p$, $2s 2p^4 4d$, $2s 2p^4 4f$, $2p^5 3s$, $2p^5 3p$, $2p^5 3d$, $2p^5 4s$, $2p^5 4p$, $2p^5 4d$ and $2p^5 4f$ resulting in 554 levels; which were subsequently included in close-coupling expansion of the scattering calculation. The energies of the low lying $2s 2p^5$ terms were much improved over the earlier reported

Table 1. A sample comparison of our theoretical energies from the 554-level model, in Rydbergs, for the first 33 levels of Ne III with the NIST [30] tabulated values.

Level No.	Configuration	Term ^a	Energy (Experiment)	Energy (Theory)	$\Delta(\%)^b$	Th. Order
1	$2s^2 2p^4$	3P_2	0.00000	0.00000	0.00	1
2	$2s^2 2p^4$	3P_1	0.00585	0.00569	2.74	2
3	$2s^2 2p^4$	3P_0	0.00839	0.00837	0.24	3
4	$2s^2 2p^4$	1D_2	0.23548	0.25804	9.58	4
5	$2s^2 2p^4$	1S_0	0.50806	0.49160	3.24	5
6	$2s^1 2p^5$	3P_2	1.86163	1.91958	3.11	6
7	$2s^1 2p^5$	3P_1	1.86694	1.92512	3.12	7
8	$2s^1 2p^5$	3P_0	1.86987	1.92791	3.10	8
9	$2s^1 2p^5$	1P_1	2.63792	2.80123	6.19	9
10	$2p^3 3s$	5S_2	2.82384	2.81852	0.19	10
11	$2p^3 3s$	3S_1	2.91087	2.91399	0.11	11
12	$2p^3 3p$	5P_1	3.17481	3.15680	0.57	12
13	$2p^3 3p$	5P_2	3.17509	3.15720	0.56	13
14	$2p^3 3p$	5P_3	3.17558	3.15781	0.56	14
15	$2p^3 3s$	3D_3	3.21799	3.21957	0.05	17
16	$2p^3 3s$	3D_2	3.21825	3.21940	0.04	16
17	$2p^3 3s$	3D_1	3.21844	3.21934	0.03	15
18	$2p^3 3p$	3P_1	3.25096	3.26061	0.30	18
19	$2p^3 3p$	3P_0	3.25105	3.26065	0.30	19
20	$2p^3 3p$	3P_2	3.25106	3.26075	0.30	20
21	$2p^3 3s$	1D_2	3.26169	3.26701	0.16	21
22	$2p^3 3s$	3P_1	3.41259	3.37052	1.23	23
23	$2p^3 3s$	3P_0	3.41260	3.37048	1.23	22
24	$2p^3 3s$	3P_2	3.41266	3.37064	1.23	24
25	$2p^3 3s$	1P_1	3.46123	3.42538	1.04	25
26	$2p^3 3p$	1P_1	3.53537	3.51826	0.48	26
27	$2p^3 3p$	3D_1	3.54523	3.52981	0.43	27
28	$2p^3 3p$	3D_2	3.54533	3.53017	0.43	28
29	$2p^3 3p$	3D_3	3.54596	3.53137	0.41	29
30	$2p^3 3p$	3F_2	3.56670	3.55916	0.21	30
31	$2p^3 3p$	3F_3	3.56684	3.55965	0.20	31
32	$2p^3 3p$	3F_4	3.56703	3.56029	0.19	32
33	$2p^3 3p$	1F_3	3.57947	3.57865	0.02	33

^a $^{2S+1}L_J$ ^b absolute percentage difference relative to NIST values

CIV3 values [26], with only the first 1D_2 level at a 9.6% difference being the greatest outlier relative to NIST energy level values [30]. A representative sample of the full 554 level calculation, is illustrated in Table 1, where it is seen that the first 33 level energies agree to within an average of 1.26% with the NIST values.

The advantage of applying the ICFT method is that the R-matrix inner region

is essentially carried out in LS coupling, including only the mass-velocity and Darwin terms. Since we are primarily focusing on line ratios between transitions within the ground state complex, we used only 20 continuum basis functions for each continuum angular momenta to keep the dimensions of the Hamiltonian matrix to a more manageable size. The inclusion of the $4p$, $4d$ and $4f$ as spectroscopic orbitals did increase the extent of the R-matrix box to 22.88 a.u, an increase of over 50% in comparison to the Breit-Pauli value. The scattering calculations were then performed with our set of parallel R -matrix programs [31, 32], which are modified versions of the serial RMATRIX I programs [33].

Partial waves with total angular momentum from $L = 0-35$ were calculated, with the Burgess-Tully top-up method used to account for higher partial wave contributions. However, considering the temperatures of astronomical interest here this should be more than sufficient to converge our excitation rates.

In the outer region, the calculation of the cross sections was split into two energy regions. Region 1 spans the energy range from the first excitation threshold up to the ionization threshold, whereas region 2 spans the energy range from from the ionization limit to four times the threshold. In region 1, for both the BP and ICFT models, we used a fine energy mesh of 40,000 points to resolve the fine Rydberg resonance structure. To account for the limited contribution of the higher partial waves to the low energy cross sections, we interpolated a coarse mesh of 200 energy points and added this to the fine mesh cross section. In region 2, above the ionisation limit, where a coarse mesh is applicable, only 200 energy points were also used for both the exchange and non-exchange calculations. The resulting total collision strengths were subsequently Maxwellian averaged across a range of electron temperatures and the effective collision strengths [34] archived for modelling. For comparison with the 56 level BP calculation, the collision strength file of the 554 level ICFT model was reduced to include only those transitions between the lowest 56 levels.

3. Collision strengths and effective collision strengths

In Fig. 3, a representative set of collision strengths for transitions within the ground state $2s^22p^4$ multiplet is given. It has been shown in previous studies, such as those of Griffin *et al.* [25] and Munoz *et al.* [3] that both ICFT and BP calculations for atomic ions should provide essentially identical results, provided that the number of terms/levels included in the configuration-interaction and close-coupling expansions are the same.

However, this is evidently not the case for the BP calculation shown in Fig. 3, as although the background collision strengths between the ICFT and the BP are similar, there are spurious resonances in the BP calculation, especially at approximately 10 Rydbergs. In fact, perhaps less obviously, for the BP model there should not be any resonance structure above 3.2 Rydbergs, as that is the last threshold included in that model. Such spurious resonances in the BP calculations would need to be removed if reliable rates are to be produced. Lastly, it should also be noted that the BP background collision strength is higher than ICFT.

The cumulative effect of these differences is reflected in the corresponding effective collision strengths [34] shown in Fig. 4. Over a wide range of electron temperatures, the 56 level BP effective collision strengths are consistently higher than the benchmark 554 level ICFT values. However, in terms of line ratios, a low density model using the coronal approximation involves the ratio of the effective collision strengths, which can

lead to smaller than expected differences in the predicted line ratios, see the results in section 4.

Figure 5 shows the $2s^22p^33s(^3S_1) \rightarrow 2s^22p^33p(^3P_{2,1,0})$ collision strengths as a function of electron energy. In this case, although small differences can be seen, the 554 levels ICFT and 56 levels BP calculations are in reasonable accord with each other. This level of agreement (i.e., $\sim 15\text{--}25\%$) was expected and typical for the collision strengths calculated as more target states are included in the scattering calculation. As anticipated, in Fig. 6, the corresponding effective collision strengths are indeed in good agreement between the two calculations.

4. Emissivity Modelling

Temperature and density sensitive energy intensity ratios between transitions among the ground state $3s^23p^4$ multiplet have been studied for Ar III [2, 3]. Here we examine the corresponding energy intensity ratios for transitions among the ground state $2s^22p^4$ multiplet of Ne III. The effective collision strengths are processed through the ADAS suite of codes (<http://www.adas.ac.uk>) with the first 5 levels in both the 56 level BP and 554 level ICFT calculation, moved to NIST energies and NIST Einstein A-coefficients where available. The NIST values are taken primarily from the work of Froese Fischer and Tachiev [35] and Kramida and Nave [36]. The wavelengths for the various transitions used in the emissivity modelling are given in figure 4.

For the temperatures and densities of interest, cascades from higher levels are not significant. Therefore, although both the ICFT and BP collisional rates include those involving the first 56 levels, only the transitions within the ground state complex are important for the following line ratios. Both datasets used the same A-values for transitions within the ground configuration.

We first examine the temperature sensitive energy intensity ratio

$$R_1 = \frac{(N_4 A_{4 \rightarrow 1} / \lambda_{4 \rightarrow 1}) + (N_4 A_{4 \rightarrow 2} / \lambda_{4 \rightarrow 2})}{N_5 A_{5 \rightarrow 4} / \lambda_{5 \rightarrow 4}} \quad (1)$$

with N_i the population in energy level i , $A_{i \rightarrow j}$ the Einstein A coefficient for a transition between energy levels i and j and $\lambda_{i \rightarrow j}$ the corresponding wavelength for the transition. Note that the index numbers for the levels are given in Table 1.

The BP and ICFT results are shown in Fig. 7. The BP and ICFT results are in good agreement with each other even though the BP effective collision strengths for these transitions were higher than the ICFT results. This is due to a cancellation of errors in the ratio. Due to the fact that the BP effective collision strengths for transitions within the ground configuration are in general higher than the ICFT ones, the BP model has increased emissivities for all of the transitions. While this does not result in a large change in the line ratios, one would see a difference when looking at absolute intensities of individual spectral lines. The results from the BP model provides larger emissivities which can affect measurements of the Ne elemental abundances, since such measurements are obtained using the absolute emissivity, or the ratio with the emissivity of a completely different ion/element. The measurements based on the BP results would lead to a lower Ne abundance.

Next we consider the density sensitive energy intensity ratio

$$R_2 = \frac{N_4 A_{4 \rightarrow 1} / \lambda_{4 \rightarrow 1}}{N_2 A_{2 \rightarrow 1} / \lambda_{2 \rightarrow 1}} \quad (2)$$

with the BP and ICFT results shown in Fig. 8. The R_2 ratio for the BP and ICFT results agree closely with each other and show a strong density dependence between electron densities of 10^4 and 10^8 cm^{-3} . As for the R_1 ratio, the R_2 ratio for Ne III shows a wider range of variation than the R_2 ratio for Ar III. Therefore, although systematically the two systems are both excellent density diagnostics, the Ne III is the marginally better option.

5. Summary

A large scale electron-impact excitation calculation of this O-like ion was carried out to investigate high energy irregularities in the cross sections of an earlier R-matrix calculation and the subsequent impact on line ratios. We have resolved these issues, and have benchmarked effective collision strengths for use in the modelling of laboratory and astrophysical plasmas. As an illustration of an application of these effective collision strengths, a study was undertaken into the viability of applying the same Ar III line ratios [3] to the Ne III case. Overall, the O-like ion, Ne III, exhibits great promise in diagnosing the temperature and density of Ne III in planetary nebulae plasmas, being more sensitive than the equivalent Ar III line ratios.

Our effective collisions strengths for the 554 level ICFT R-matrix calculation shall be made available on the Oak Ridge National Laboratory Atomic Data website (http://www-cfadc.phy.ornl.gov/data_and_codes) and in the ADAS database (<http://www.adas.ac.uk>).

6. Acknowledgements

It is a pleasure to thank Professor A Dalgarno FRS, for drawing our attention to this problem and the need for accurate atomic data required for the modelling of planetary nebulae. T-G Lee, C P Ballance and J A Ludlow were supported by US Department of Energy (DoE) grants through Auburn University. E Landi acknowledges support from NASA grants NNX10AM17G and NNX11AC20G. B M McLaughlin acknowledges support by the US National Science Foundation through a grant to ITAMP at the Harvard-Smithsonian Center for Astrophysics. The computational work was carried out at the National Energy Research Scientific Computing Center in Oakland, CA, USA and on the Tera-grid at the National Institute for Computational Sciences (NICS) in Knoxville, TN, USA, which is supported in part by the US National Science Foundation.

References

- [1] De Robertis M M, Dufour J R and Hunt R W 1987 *J. Roy. Astron. Soc. Can.* **81** 195
- [2] Keenan F P and Conlon E S 1993 *Astrophys. J.* **410** 426
- [3] Munoz Burgos J M, Loch S D, Ballance C P and Boivin R F 2009 *Astronomy and Astrophysics* **500** 1253
- [4] Simpson J P, Colgan S W J, Rubin R H, Erickson E F and Haas M R 1995 *Astrophys. J.* **444** 721
- [5] Rubin R H, Simpson J P, Haas M R and Erickson E F 1991 *Astrophys. J.* **374** 564
- [6] Baldwin J A, Ferland G J, Martin P G, Corbin M R, Cota S A, Peterson B M and Slettebak A 1991 *Astrophys. J.* **374** 580
- [7] Colgan S W J, Haas M R, Erickson E F, Rubin R H, Simpson J P and Russell R W 1993 *Astrophys. J.* **413** 237

- [8] Minkowski R Radio Astronomy. In: H.C. Van de Hulst, Editor, IAU Symp. vol. 4, Cambridge University, Cambridge (1957), p. 107
- [9] Fesen R A 1990 *Astrophys. J.* **99** 1904
- [10] Persson W, Wahlström C-G, Jönsson L and Di Rocco H O 1991 *Phys. Rev. A* **43** 4791
- [11] James G K, Kanik I and Ajello J M 1995 *Astrophys. J.* **455** 769
- [12] Daw A, Parkinson W H, Smith P L and Calamai A G 2000 *Astrophys. J.* **533** L179
- [13] Clegg R E S, Storey P J and Harrington J P 1986 *Mon. Not. R. Astron. Soc.* **221** 61
- [14] McLaughlin B M and Bell K L 2000 *J. Phys. B: At. Mol. Opt. Phys.* **33** 597
- [15] Seaton M J 1953 *Proc. R. Soc. A* **218** 355
- [16] Seaton M J 1955 *Proc. R. Soc. A* **264** 400
- [17] Seaton M J 1958 *Rev. Mod. Phys.* **30** 979
- [18] Blaha M 1968 *Ann. Astrophys.* **31** 311
- [19] Czyzak S J, Kruger T K, Saraph H E and Shemming J 1967 *Proc. Phys. Soc.* **92** 1146
- [20] Pradhan A K 1974 *J. Phys. B: At. Mol. Opt. Phys.* **17** L503
- [21] Butler K and Mendoza C 1984 *Mon. Not. Roy. Astron. Soc.* **208** 17
- [22] Saraph H E 1978 *Comput. Phys. Commun.* **15** 247
- [23] Saraph H E and Eissner W *Comput. Phys. Commun.*, to be published.
- [24] McLaughlin B M, Daw A and Bell K L 2002 *J. Phys. B: At. Mol. Opt. Phys.* **35** 283
- [25] Griffin D C, Badnell N G and Pindzola M S 1998 *J. Phys. B: At. Mol. Opt. Phys.* **31** 3713
- [26] Hibbert A 1975 *Comput. Phys. Commun.* **11** 141
- [27] See, <http://vanadium.rollins.edu/GASP/GASP.html>
- [28] Badnell N R 1997 *J. Phys. B: At. Mol. Opt. Phys.* **30** 1
- [29] Landi E and Bhatia A K 2005 *At. Data and Nucl. Data Tables* **89** 195
- [30] Ralchenko Y, Kramida A E, Reader J, and NIST ASD Team (2011), NIST Atomic Spectra Database, National Institute of Standards and Technology, Gaithersburg, MD, USA (<http://physics.nist.gov/asd3>)
- [31] Mitnik D M, Griffin D C, Ballance C P and Badnell N R 2003 *J. Phys. B: At. Mol. Opt. Phys.* **36** 717
- [32] Ballance C P and Griffin D C 2004 *J. Phys. B: At. Mol. Opt. Phys.* **37** 2943
- [33] Berrington K A, Eissner W and Norrington P H 2005 *Comput. Phys. Commun.* **92** 290
- [34] Eissner W, Martins P de A P, Nussbaumer H, Saraph H E and Seaton M 1969 *Mon. Not. R. Astron. Soc.* **146** 63
- [35] Froese Fischer C and Tachiev G 2004 *At. Data Nucl. Data Tables* **87** 1
- [36] Kramida A E and Nave G 2006 *Eur. Phys. J D* **37** 1

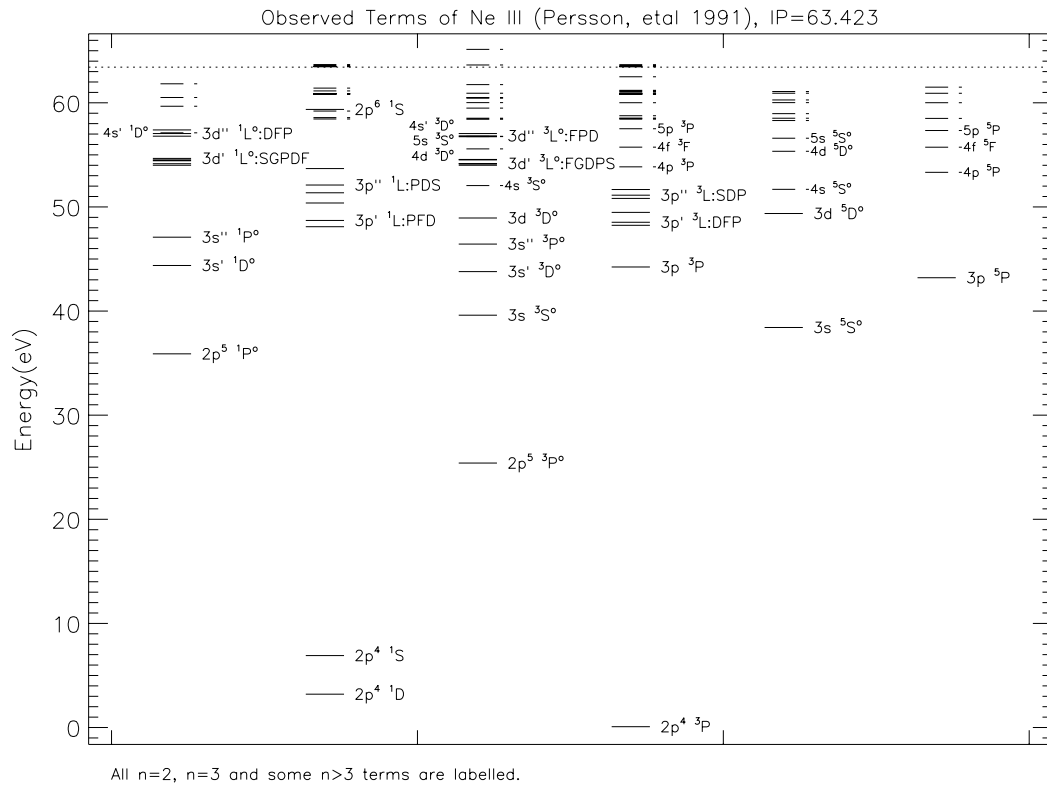


Figure 1. Ne III, energy level diagram (levels given in eV) showing the observed low lying levels of NeIII from the laboratory work of Persson *et al.* [10].

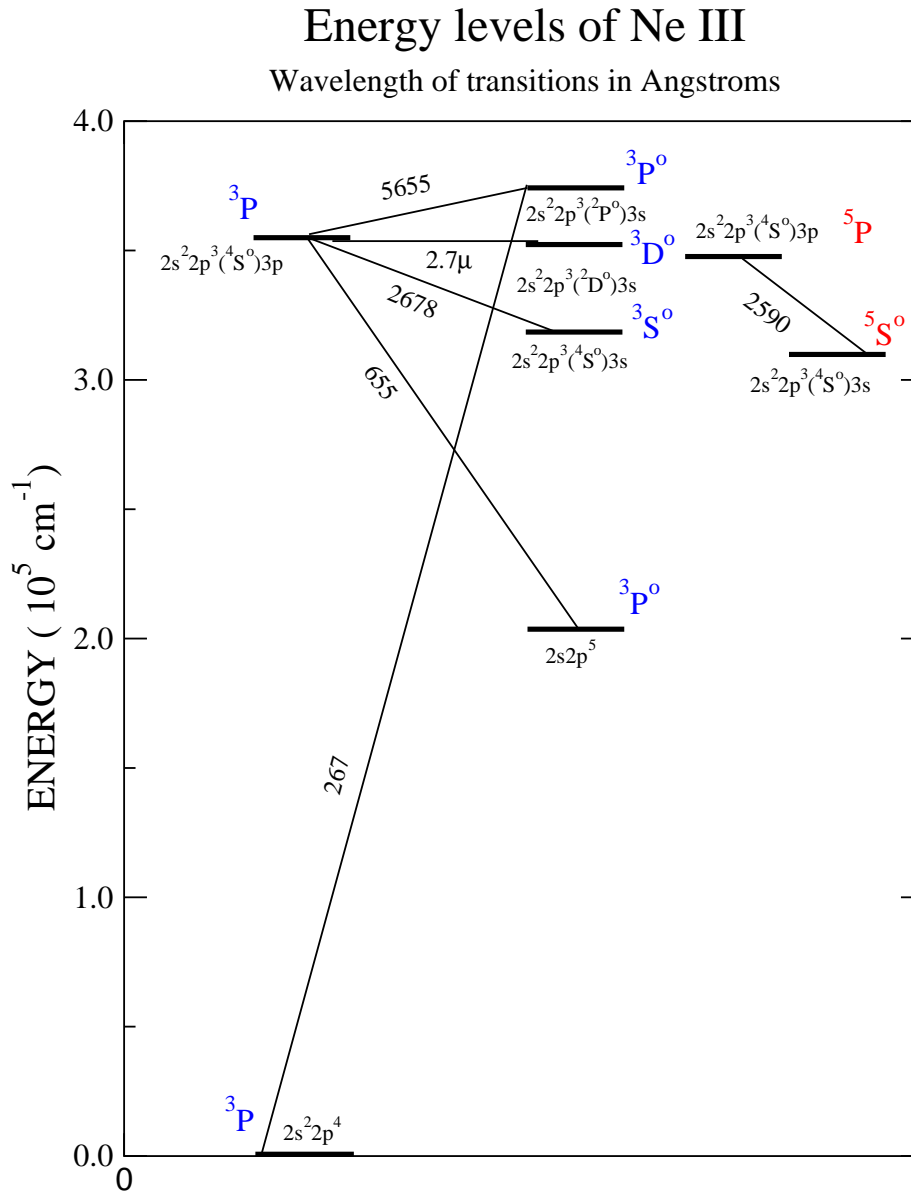


Figure 2. (Colour online) An overview of energy levels (levels given in cm^{-1}) illustrating the transitions of interest in the planetary nebulae NGC 3918 [13] for Ne III. The wavelength of the astrophysically observed transitions are labelled in units of Angstroms. For multiplets, the wavelength (in \AA) of the strongest observed lines is given. Singlet levels are omitted for clarity.

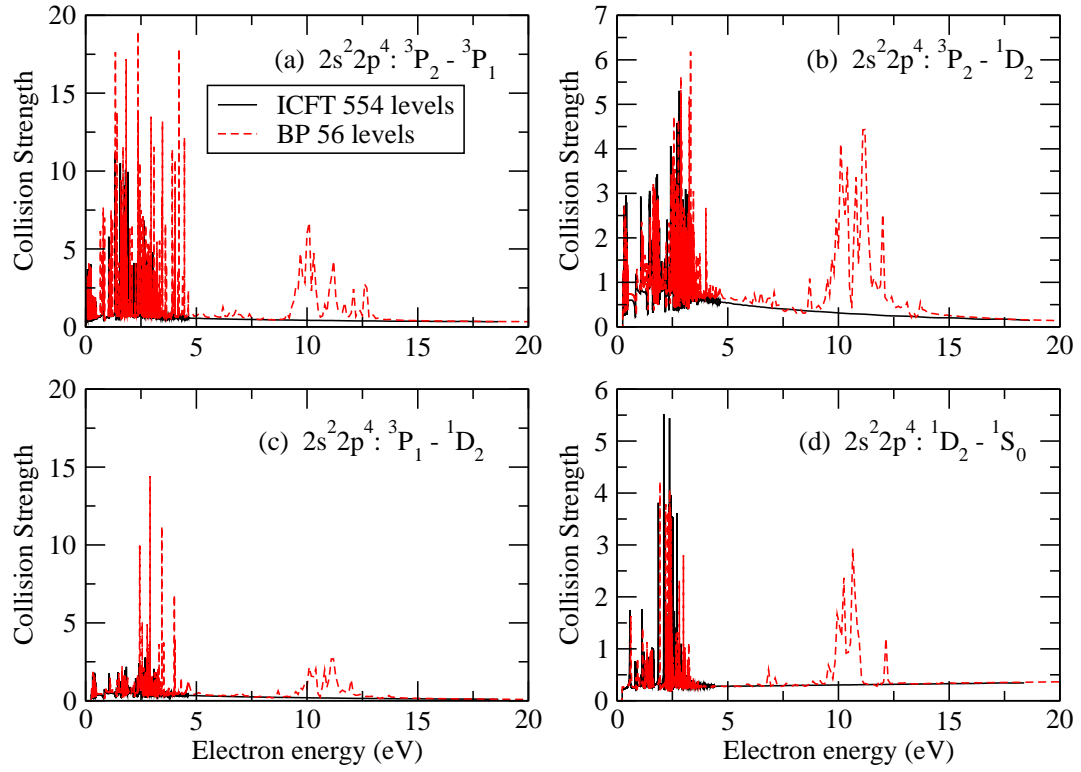


Figure 3. (Colour online) Collision strengths for the transitions (a) $2s^2 2p^4 : ^3P_2 - ^3P_1$, (b) $2s^2 2p^4 : ^3P_2 - ^1D_2$, (c) $2s^2 2p^4 : ^3P_1 - ^1D_2$ and (d) $2s^2 2p^4 : ^1D_2 - ^1S_0$ as a function of the incident electron energy. The solid black line indicates the 554 level ICFT results and the dashed red line indicates the 56 level Breit-Pauli results.

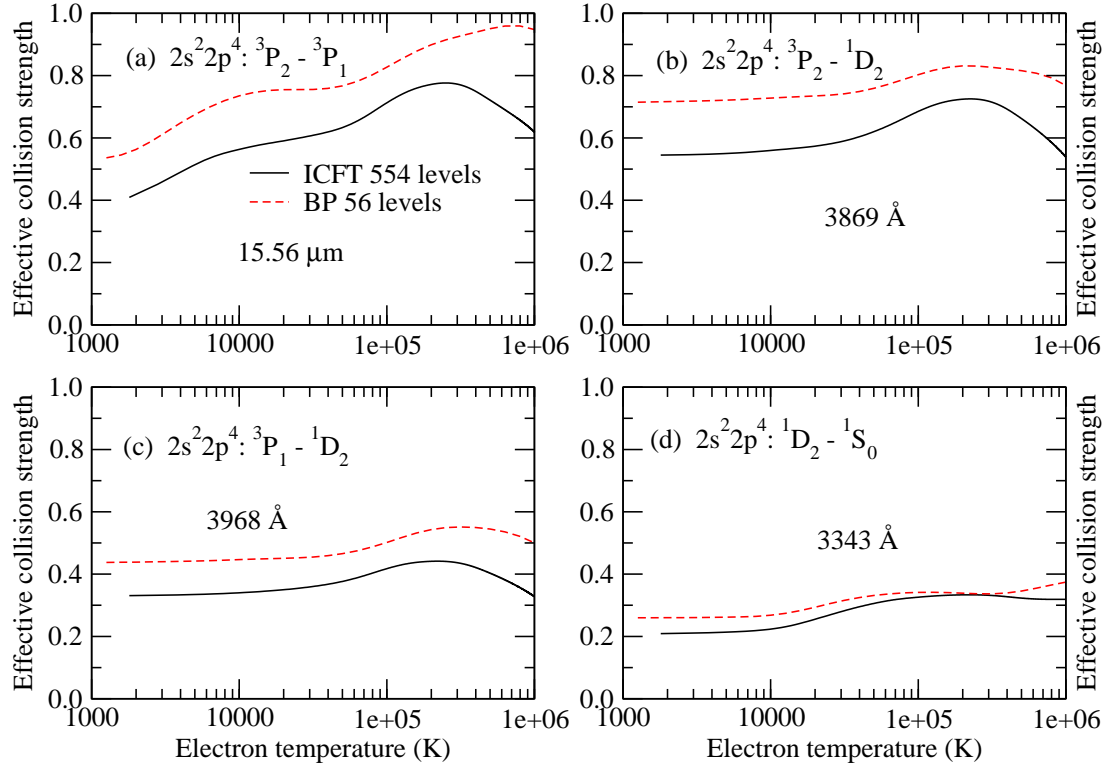


Figure 4. (Colour online) Effective collision strengths obtained by averaging the collision strengths over a Maxwellian temperature distribution for the electrons. Results are shown for the transitions (a) $2s^2 2p^4 : ^3P_2 - ^3P_1$, (b) $2s^2 2p^4 : ^3P_2 - ^1D_2$, (c) $2s^2 2p^4 : ^3P_1 - ^1D_2$ and (d) $2s^2 2p^4 : ^1D_2 - ^1S_0$ as a function of the electron temperature (K). The solid black line indicates the 554 level ICFT results and the dashed red line indicates the 56 level Breit-Pauli results. The wavelengths in Angstroms for the various transitions are also included for completeness

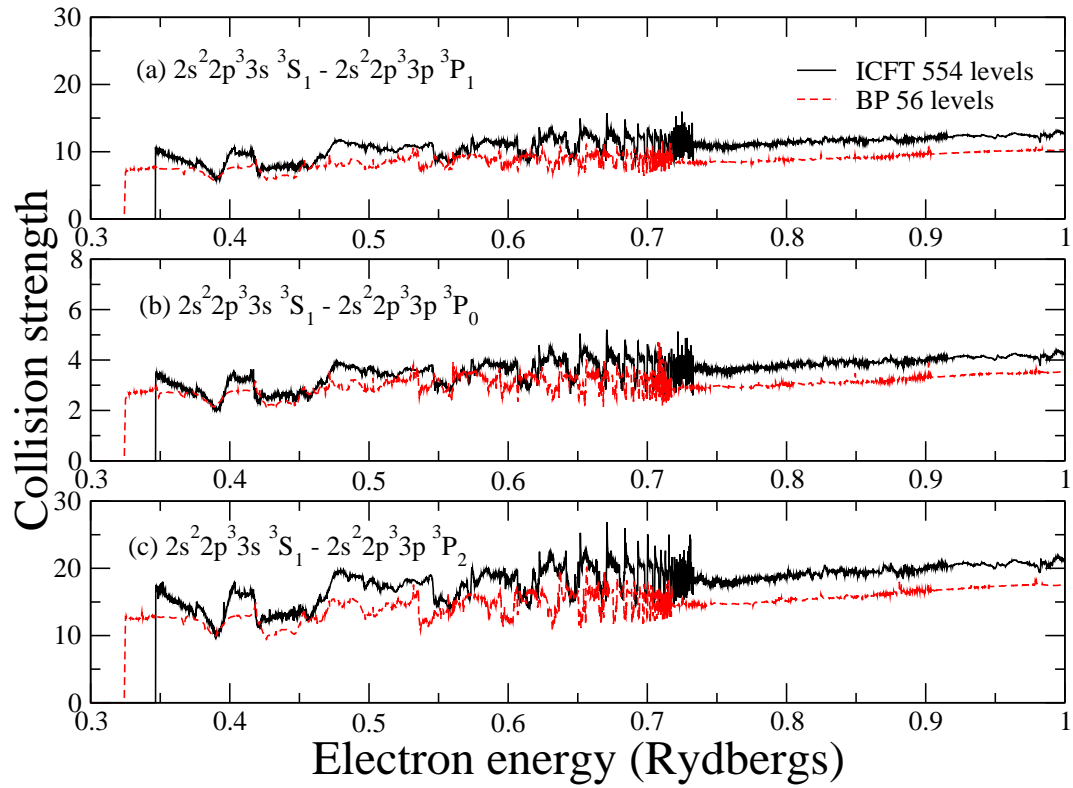


Figure 5. (Colour online) Collision strengths for the transitions (a) $2s^2 2p^3 3s^3 S_1 - 2s^2 2p^3 3p^3 P_1$, (b) $2s^2 2p^3 3s^3 S_1 - 2s^2 2p^3 3p^3 P_0$, (c) $2s^2 2p^3 3s^3 S_1 - 2s^2 2p^3 3p^3 P_2$ as a function of the incident electron energy. The solid black line indicates the 554 level ICFT results and the dashed red line indicates the 56 level Breit-Pauli results.

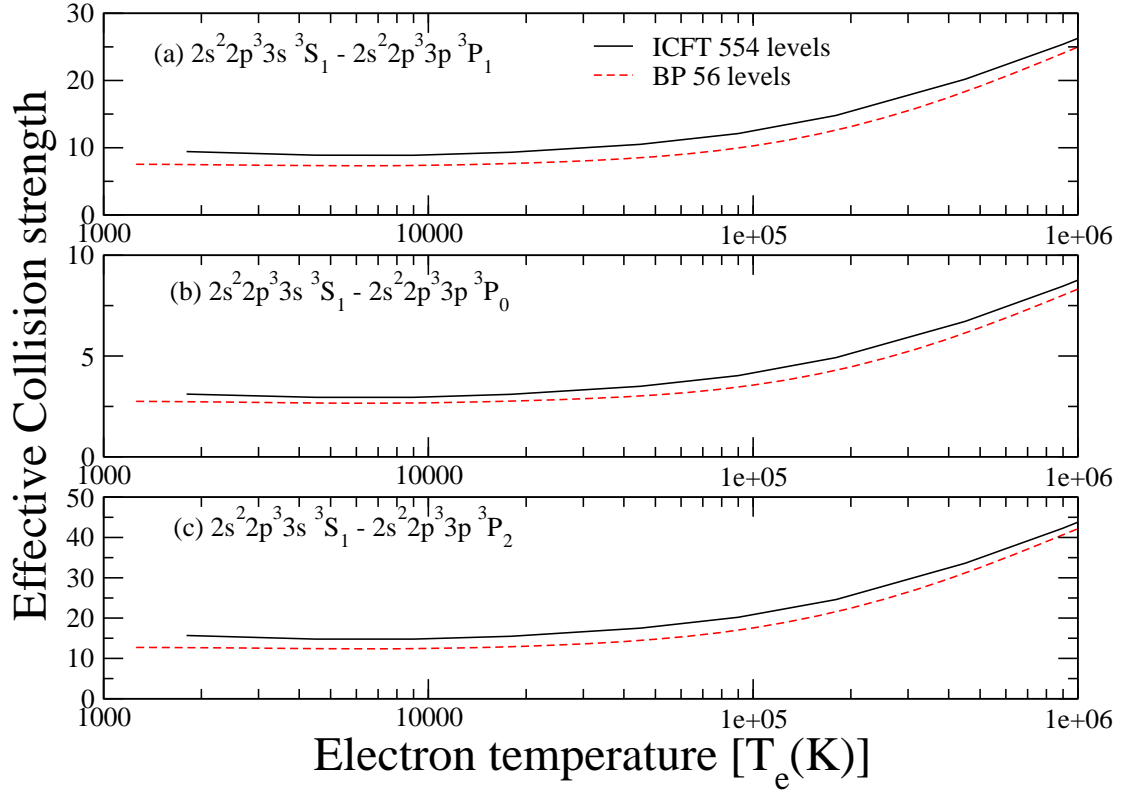


Figure 6. (Colour online) Effective collision strengths obtained by averaging the collision strengths over a Maxwellian temperature distribution for the electrons. Results are shown for the transitions (a) $2s^2 2p^3 3s^3 S_1 - 2s^2 2p^3 3p^3 P_1$, (b) $2s^2 2p^3 3s^3 S_1 - 2s^2 2p^3 3p^3 P_0$, (c) $2s^2 2p^3 3s^3 S_1 - 2s^2 2p^3 3p^3 P_2$ as a function of the electron temperature (K). The solid black line indicates the 554 level ICFT results and the dashed red line indicates the 56 level Breit-Pauli results.

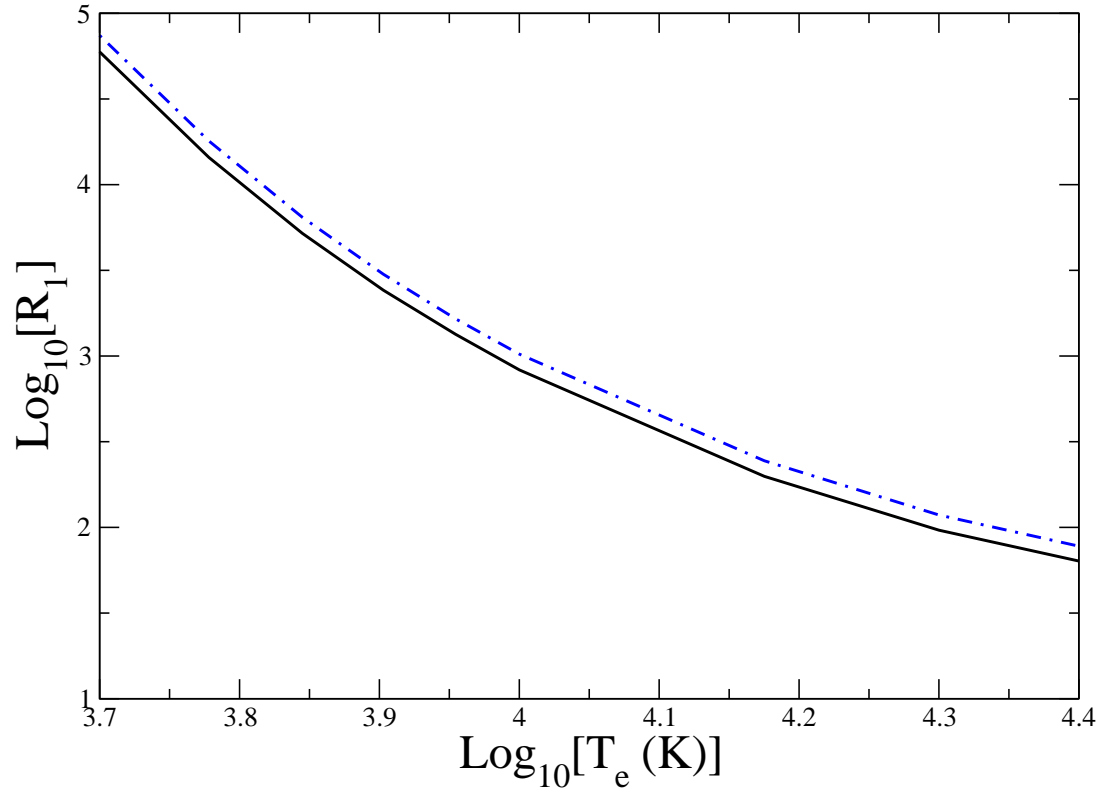


Figure 7. (Colour online) R_1 line ratio as a function of electron temperature for an electron density of $N_e = 1 \times 10^3 \text{ cm}^{-3}$. The solid black line shows the results using the 554 level ICFT R-matrix calculation and the dot-dashed blue line shows the result using the 56 level Breit-Pauli R-matrix calculation, with the energies and transition rates for the first 5 levels in both R-matrix calculations shifted to NIST energies and transition rates[30] for the modelling calculations.

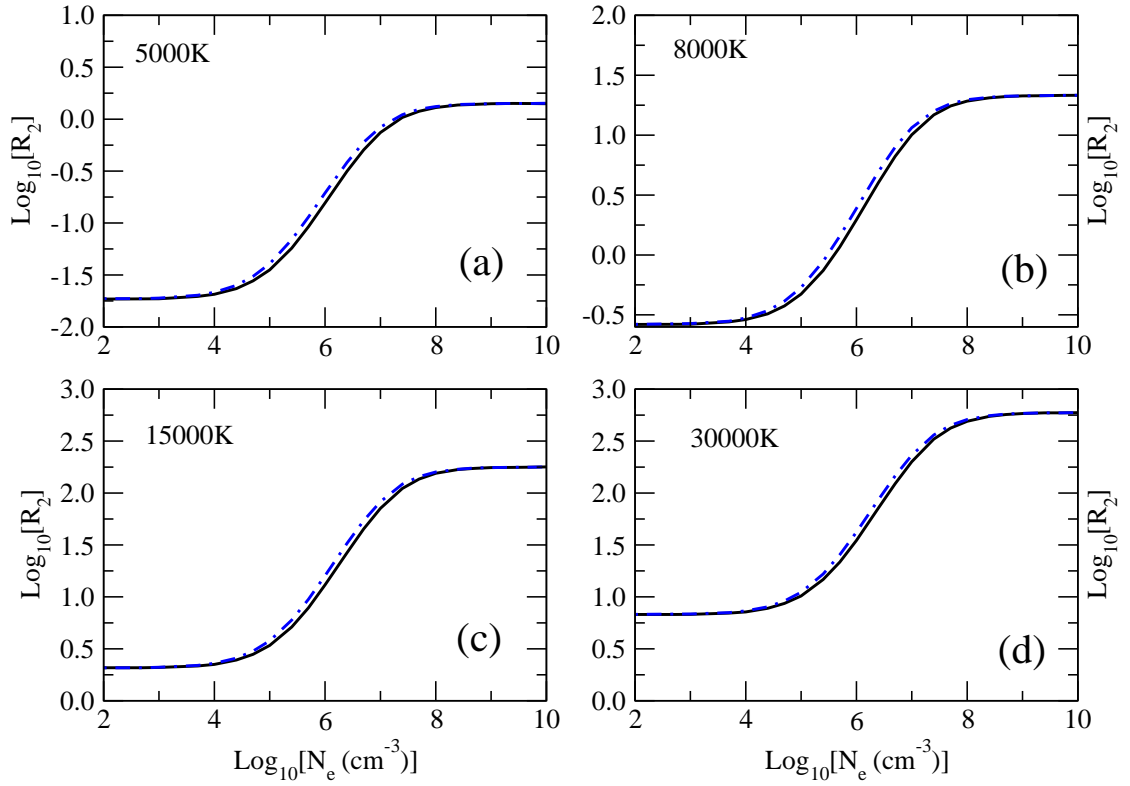


Figure 8. (Colour online) R_2 line ratio as a function of electron density for electron temperatures of (a) 5000K (b) 8000K (c) 15000K, and (d) 30000K. The solid black line shows the results using the 554 level ICFT R-matrix calculation and the dot-dashed blue line shows the result using the 56 level Breit-Pauli R-matrix calculation.